A density functional LCAO embedded-cluster calculation on the Jahn-Teller distorted states of H^{2-} in CaO crystal

1995 J. Phys.: Condens. Matter 7 9625

(http://iopscience.iop.org/0953-8984/7/49/024)

J. Phys.: Condens. Matter 7 (1995) 9625–9633. Printed in the UK

A density functional LCAO embedded-cluster calculation on the Jahn–Teller distorted states of H^{2-} in CaO crystal

S C Ke, D C Patton, J G Harrison and H T Tohver

Physics Department, University of Alabama at Birmingham, Birmingham, AL 35294, USA

Received 19 June 1995, in final form 8 August 1995

Abstract. To address recent electron paramagnetic resonance experiments showing a distortion at the H^{2-} site lowering the defect symmetry from cubic to tetragonal in CaO crystal, we have investigated the defect-induced lattice relaxation of an H^{2-} ion in CaO with local O_h and D_{4h} symmetry respectively using a first-principles embedded-cluster approach based on the local density approximation of density functional theory. We show that the ground state in O_h symmetry is an orbitally degenerate t_{1u} state, while in D_{4h} symmetry it is an a_1 state. This Jahn–Teller distortion of the CaO:H^{2-} system is consistent with the experimental findings. We find that the position of the HOMO t_{1u} root in the bandgap is sensitive to the inclusion of the 3d orbital at the nearest-neighbour Ca^{2+} sites suggesting a bonding interaction. The Fermi contact spin density at the proton is in good agreement with the observed values, while a significant discrepancy is found at the Ca^{2+} sites. Mulliken analysis indicates that the spin density at the proton is mainly due to the core polarization of the H^{2-} 1s orbital.

1. Introduction

Considerable experimental progress has been made in understanding the properties of hydrogen H^{2-} ion in thermochemically reduced MgO [1, 2] and CaO [3–5]. It has been shown that the H^- ions (a proton with two electrons) present substitutionally at oxygen vacancy sites can act as traps for electrons photoexcited from F centres, resulting in F^+ and H^{2-} centres [3]. The H^{2-} ions are metastable at room temperature; the trapped electrons are subsequently released by thermal activation resulting in the reverse process and leading to F centre luminescence. Recently, the defect configuration of H^{2-} in CaO has attracted a great deal of interest due to the report of symmetry lowering of the hydrogen electron paramagnetic resonance (EPR) spectrum [4]. The H^{2-} ion in CaO is paramagnetic and has an isotropic EPR spectrum above 13 K. At 4 K, the defect symmetry is tetragonal with ⟨001⟩ as the symmetry axis; an [H^-Ca^+] model to account for the symmetry lowering was proposed by Orera *et al* [4]. Their model is one in which the unpaired electron is localized in the 4s orbital of one of the calcium sites surrounding the substitutional H^- ion. However, the EPR spectrum of H^{2-} ions in a stressed sample at 13 K reveals the same symmetry and spin-Hamiltonian parameters as of unstressed samples at 4 K [5]. Furthermore, the observation of axial superhyperfine splitting by the ^{43}Ca nucleus of the hydrogen EPR signal has unambiguously shown that the defect configuration is a proton with three electrons in the oxygen vacancy [5]. On the basis of the EPR results, a T_{1u} ground state with the threefold degeneracy removed by a tetragonal Jahn–Teller distortion of the lattice was proposed as the defect model of H^{2-} centres in CaO [5].

0953-8984/95/499625+09$19.50

That the ground state of an H^{2-} ion in a cubic unrelaxed CaO host is of the orbitally degenerate t_{1u} type was proposed independently by Hsu [6] and Rõõm [7], using LSDA and X_α multiple scattering methods, respectively. However, the energy level and the equilibrium atomic positions are both strongly affected by the presence of defect-induced relaxation. Hence, it is more appropriate to include the relaxation of bulk crystal atoms around the defect in the point defect properties calculation. The purpose of this paper is to supplement our previous EPR investigations of the H^{2-} ion in CaO, and focus on the role of the Jahn–Teller distortion by performing a first-principles embedded-cluster calculation. The calculation is based on the local density approximation, and the symmetry-constrained atomic shells in the defect cluster are allowed to relax.

We first describe the cluster embedding mechanism and automated quasidynamical procedure in updating the atomic positions. In section 3, guided by previous experimental results, we propose our calculation procedures. In section 4 we present the results of calculations of an embedded H^{2-} ion in CaO with local O_h and D_{4h} symmetry respectively. Comparisons are drawn between the calculated and experimental results. In section 5, we discuss the properties of the highest occupied level and the spin densities at the nuclear sites.

2. Computational approach

Our calculations are based on density functional theory within the Kohn–Sham local density approximation (LDA) [8], using the linear combination of Gaussian orbitals method. In the LDA, the total energy of the ground state of an N-electron system has the usual form [9]. However, for the one-electron potential V_{ext} (equation (1)), we add the host Madelung potential V_{host} arising from cluster embedding to the Coulomb potential of the nuclei with atomic number Z_v centred at R_v:

$$V_{ext} = -\sum_v \frac{Z_v}{|r - R_v|} + V_{host}. \tag{1}$$

To evaluate the cluster embedding potential V_{host} at a mesh point, we subtract the Madelung potential due to the cluster from that due to the infinite crystal (see figure 1); the Madelung potential is evaluated by the method of F C Frank [10]. We add the Ceperley–Alder correlation functional to the Kohn–Sham exchange functional. The level of convergence of the LDA total energy is roughly 10^{-3} au.

The LDA calculations of the localized H^{2-} impurity in the CaO system are performed for a 33-atom cluster, which includes a central hydrogen atom and the (100), (110), (111), and (200) near-neighbour shells. The inclusion of the (200) shell serves somewhat as a bulk boundary condition to the relaxed (100) shell. To augment the variational freedom of the basis, extensive basis functions are used for the hydrogen atom and atoms at the first two shells—(100) and (110). They consist of four Gaussian orbitals which are contracted to 1s, 2s, plus two p-type single Gaussian orbitals for hydrogen atom; 14 Gaussian orbitals contracted to 1s, 2s, 3s, 2p, 3p, 3d, plus two s-like and two p-like single Gaussian orbitals for each Ca atom at the (100) shell; and 12 Gaussian orbitals contracted to 1s, 2s, 2p, plus two s-like and one p-like single Gaussian orbitals for each O atom at the (110) shell. Minimal basis sets are used for (111) and (200) shells.

To update the atomic geometries of the cluster in consecutive LDA energy calculations, atomic forces [11] are calculated based on the usual Hellmann–Feynman theorem incorporated with basis set corrected forces. The geometry optimization is performed automatically, using the calculated atomic forces by a conjugate-gradient-based algorithm.

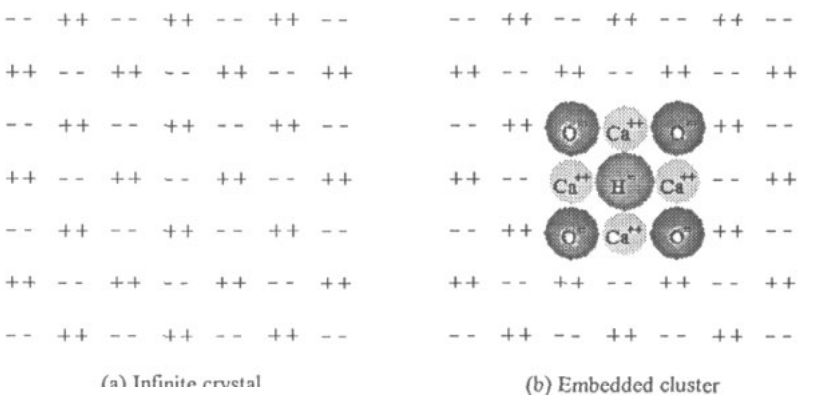

Figure 1. The cluster embedding mechanism for (a) infinite crystal of divalent CaO structure. To calculate the Madelung potential, the lattice points are replaced by positive and negative point charges. (b) A $Ca_{14}O_{13}H$ cluster embedded in the infinite crystal.

Because of the possibilities of local minima in the total energy surface, we choose a variety of starting geometries to minimize the possibility of bias toward one of these local minima. To investigate the lowest-energy configuration (LDA ground state), we start with the experimental geometry and allow the automated geometry optimization mechanism to proceed until a local energy minimum is found; we then repeat this procedure for a series of appropriate nuclear geometry inputs. The LDA total energy surface is then expressible as a function of nuclear coordinates. We choose the overall lowest local minimum as the global minimum.

3. Calculation procedures

We first calculate the LDA total energy of a $CaO:H^{2-}$ embedded cluster of O_h symmetry because part of the interpretation of the experimental results was based on the assumption that the ground state in O_h symmetry is of orbitally degenerate t_{1u} type.

The symmetric part of the product $T_{1u} \times T_{1u}$ contains A_{1g}, E_g, and T_{2g} irreducible representations of O_h. The A_{1g} mode does not induce splitting of the electronic states. Hence, depending on the relative coupling strength of the E_g and T_{2g} modes, two types of static Jahn–Teller distortion are possible, tetragonal and trigonal deformation of the H^{2-} ion surroundings respectively. Analysis of the EPR spectra [5] shows that only a spontaneous tetragonal distortion occurred at the H^{2-} site. Therefore only a tetragonal distorted lattice is considered in the reduced-symmetry calculations. It is then of interest to determine which sign of the tetragonal distortion is preferred since both $Q_3 > 0$ (elongation along the tetragonal axis) and $Q_3 < 0$ (contraction along the tetragonal axis) modes belong to the E_g irreducible representation.

The reduced-symmetry calculations consist of: (1) the first (001) and second (100) near-neighbour shells are allowed to relax while the remaining atoms stay fixed, (2) all shells are allowed to relax. Both relaxation processes are constrained by D_{4h} symmetry.

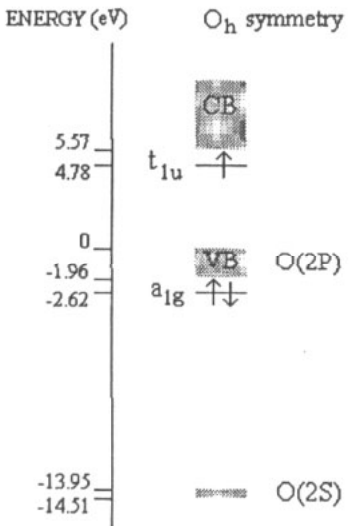

Figure 2. The energy levels of H^{2-} in CaO. The energy is measured relative to the top of the oxygen 2p valence band. The bottom of the conduction band is taken as the lowest unoccupied level in a pure CaO cluster. The reduction of the calculated band gap of 5.57 eV, compared with experimentally obtained value of 7.03 eV [14], is a consequence of the local density approximation [7, 15].

4. Results

4.1. O_h symmetry

The calculations are performed on a cluster with 14 Ca atoms, 18 O atoms and a proton with three electrons in the centre of inversion symmetry (oxygen vacancy). All 33 atoms in the cluster are fully relaxed in accordance with the method described in section 2. Based on 11 total-energy calculations, the minimum-energy structure is found to be $a = 4.623$ au, $b = 4.593$ au, $c = 4.092$ au, and $d = 4.531$ au, where the first atomic shell is at $a(100)$, the second at $b(110)$, the third at $c(111)$ and the fourth at $d(200)$. The nearest shell relaxed inwards towards the H^{2-} ion by 1.0%, and the second-nearest shell relaxed inwards by 0.6% compared with the calculated atomic spacing in a pure CaO cluster. For a pure CaO cluster, the calculated minimum-energy geometry is $a = 4.672$ au, $b = 4.621$ au, $c = 4.029$ au, and $d = 4.533$ au. This result is unusual as one would expect the opposite for a substitutional ion with larger ionic radius than the pure lattice ion, at least 1.54 Å for H^{2-} versus 1.32 Å for O^{2-} [12]. This result reflects the smallness of the replusive core as compared to the full ionic radius.

It is important to note that the highest occupied level in the defect cluster is of t_{1u} character for all the 11 total-energy calculations. To investigate the convergence of the t_{1u} level, we first add a long-range d-like single Gaussian orbital to the nearest-neighbour calcium sites. Then we gradually remove basis functions; the corresponding eigenvalues of the t_{1u} level are listed in table 1 showing that the level of the highest occupied t_{1u} state has converged. The eigenvalue of the 3d atomic orbital of Ca^{2+} is -0.852 au; in this case we use the atomic SIC-LSDA [13] method. Taking 1.74 as the Madelung constant of CaO and 4.528 as the nearest-neighbour distance yields Madelung potential of 0.729 au at the Ca^{2+} site in the divalent CaO crystal. Hence, the energy of the 3d level is equal to -0.123 au

(−3.34 eV). This estimation places the level of the Ca^{2+} 3d level in the vicinity of the t_{1u} state. This suggests that the position of the t_{1u} level as being the highest occupied level is largely due to bonding type interaction with the 3d-like state of Ca^{2+} ions.

Table 1. Eigenvalues of the highest occupied level as a function of basis set.

Basis at (100) Ca^{2+} sites	*Eigenvalues (eV)*	*Symmetry*
Minimal = 1s+2s+3s +2p +3p	−3.21	t_{1u}
Minimal + one s-like SGOs	−3.27	t_{1u}
Minimal + two s-like SGOs	−3.22	t_{1u}
Minimal + two s and one p-like SGOs	−3.22	t_{1u}
Minimal + two s and two p-like SGOs	−3.47	t_{1u}
Minimal + two s and two p-like SGOs+ 3d(atomic)†	−3.86	t_{1u}
Minimal + two s and two p-like SGOs+ 3d(atomic) + one d-like SGOs	−3.88	t_{1u}

† Optimal basis set.

The orbital energy level scheme for the minimum energy structure is depicted in figure 2. Our Mulliken analysis shows that the first two electrons of the H^{2-} ion are located on the $2a_{1g}$ orbital (hydrogen 1s-like orbital) which lies below the oxygen 2p-like valence band; and the highest singly occupied orbital is $5t_{1u}$ which lies 0.79 eV below the conduction band. Three points of agreement can be found between experiment and the present results: (1) The fully occupied $2a_{1g}$ orbital indicates that for a hydrogen defect in CaO the proton is always filled with at least two electrons— hence, no EPR signal due to atomic hydrogen should be observed [7]; (2) the highest occupied $5t_{1u}$ orbital is close to the conduction band bottom—that is, in agreement with the infrared absorption results of Orera *et al* [3] showing that the H^{2-} defects are the main traps for electrons excited from F centres and responsible for the long-lived luminescence in CaO; the experimentally [3] inferred value for the H^{2-} defect level is 0.73 eV below the conduction band at 77 K; (3) with the orbitally degenerate t_{1u} as the ground state in O_h symmetry, the system would be Jahn–Teller unstable as suggested in [5].

4.2. D_{4h} symmetry

From O_h to D_{4h} symmetry, the atomic shells surrounding the substitutional H^{2-} ion break into $a(001)$ and $b(100)$ calcium shells, $c(110)$ and $d(101)$ oxygen shells, $e(111)$ calcium shells, plus $f(002)$ and $g(200)$ oxygen shells; each shell consists of 2, 4, 4, 8, 8, 2, and 4 atoms, respectively.

4.2.1. Relaxation of the first two shells. To investigate symmetry-breaking distortion modes, we chose a range of initial geometries by moving the calcium atoms of the first two shells (a and b) along the tetragonal symmetry axis, ranging from ±2% to ±12% of the experimental Ca–O bond length. The atomic geometries of shells a and b are then optimized for each set of inputs in accordance with the method described in section 2. The remaining five shells are held fixed at the experimental bond length of 2.4 Å. Figure 3(a) displays the LDA energy surface generated from a spline interpolation to the 54 calculated total energy points. Figure 3(c) shows a slice of the three-dimensional surface in a direction that connects the starting geometry (O_h) and the minimum-energy configuration. The minimum-energy cluster configuration is found to be at $a = 5.152$ au and $b = 4.681$ au. The ratio a/b of 1:10 indicates that elongation rather than contraction along the tetragonal axis of the

octahedron is preferred for H^{2-} ions in CaO. This is in qualitative agreement with the EPR results [5].

4.2.2. All atoms relaxed. To further investigate the LDA ground state, we allow the whole 33-atom cluster to relax to its full variational ground state to counteract more efficiently the effects of truncating the cluster at a finite size. The lattice relaxation process is similar to that discussed above. Based on 51 calculated total energy points, we find the minimum energy structure to be at $a = 5.067_5$ and $b = 4.575$. The ratio of a/b is equal to 1:11, consistent with above result of 1:10. The energy of the relaxed $Ca_{14}O_{18}H$ system in D_{4h} symmetry is 6.87 eV lower than that of the relaxed system in O_h symmetry.

5. Discussion

As a result of Jahn–Teller distortion, the orbitally degenerate t_{1u} ground state (O_h symmetry) breaks into a_{1g} and e_g-type orbitals; and the highest occupied level in D_{4h} symmetry is of a_1 character. The Mulliken population of the highest occupied level of H^{2-} in CaO is listed in table 2. It appears that the H^{2-} ground state orbital is mainly an admixture of the hydrogen 2p and nearest-neighbour calcium 3d orbitals. The Mulliken analysis of the charge distribution assigns 10% and 30% of electron charges to the first two calcium shells, respectively, due to the mixing of H (2p) and Ca (3d) orbitals. It also indicates that the ground state wavefunction does not extend outside the cluster. The electron delocalization of the H^{2-} ground state in the cluster is consistent with the experimental finding of the low threshold energy (0.2 eV) for the optical destruction of the H^{2-} centre [7].

Table 2. Charge distribution of the highest occupied level.

	Charge distribution							
Symmetry	H(000)	Ca(100)		O(110)		Ca(111)	O(200)	
O_h	0.46	0.48		0.04		0	0.02	
Symmetry	H(000)	Ca(001)	Ca(100)	O(110)	O(101)	Ca(111)	O(002)	O(200)
D_{4h}	0.48	0.11	0.31	0	0.06	0	0.01	0
Orbital character	p	3d		2p		—	2p	

It is interesting to compare our calculated results for the H^{2-} centres in CaO with those for MgO. In MgO, the H^{2-} ground state in O_h symmetry as a diffuse a_{1g}-type orbital spreading beyond the third-nearest-neighbour shell of ions was proposed by Tombrello *et al* [2] based on the open-shell Hartree–Fock–Rothaan procedure with a seven atom cluster; by Vail [16] based on the ICECAP procedure with an embedded nearest-neighbour cluster; and by Rõõm [7] using the X_α multiple-scattering method with a 27-atom cluster. However, a t_{1u} ground state of H^{2-} in MgO (O_h) was suggested by Hsu [6], utilizing the LSDA in an embedded 27-atom cluster. According to Hsus analysis [6], the different results can be accounted for by the truncation of the cluster at a finite size and the cluster embedding effects as well as the inclusion of long-range single Gaussian orbitals at the nearest-neighbour magnesium sites.

Another parameter to be compared with the EPR results is the spin density at the nucleus. For H^{2-} in CaO, we find the spin density at the proton calculated in a relaxed embedded cluster is 270×10^{20} and 283×10^{20} cm^{-3} for O_h and D_{4h} symmetry, respectively.

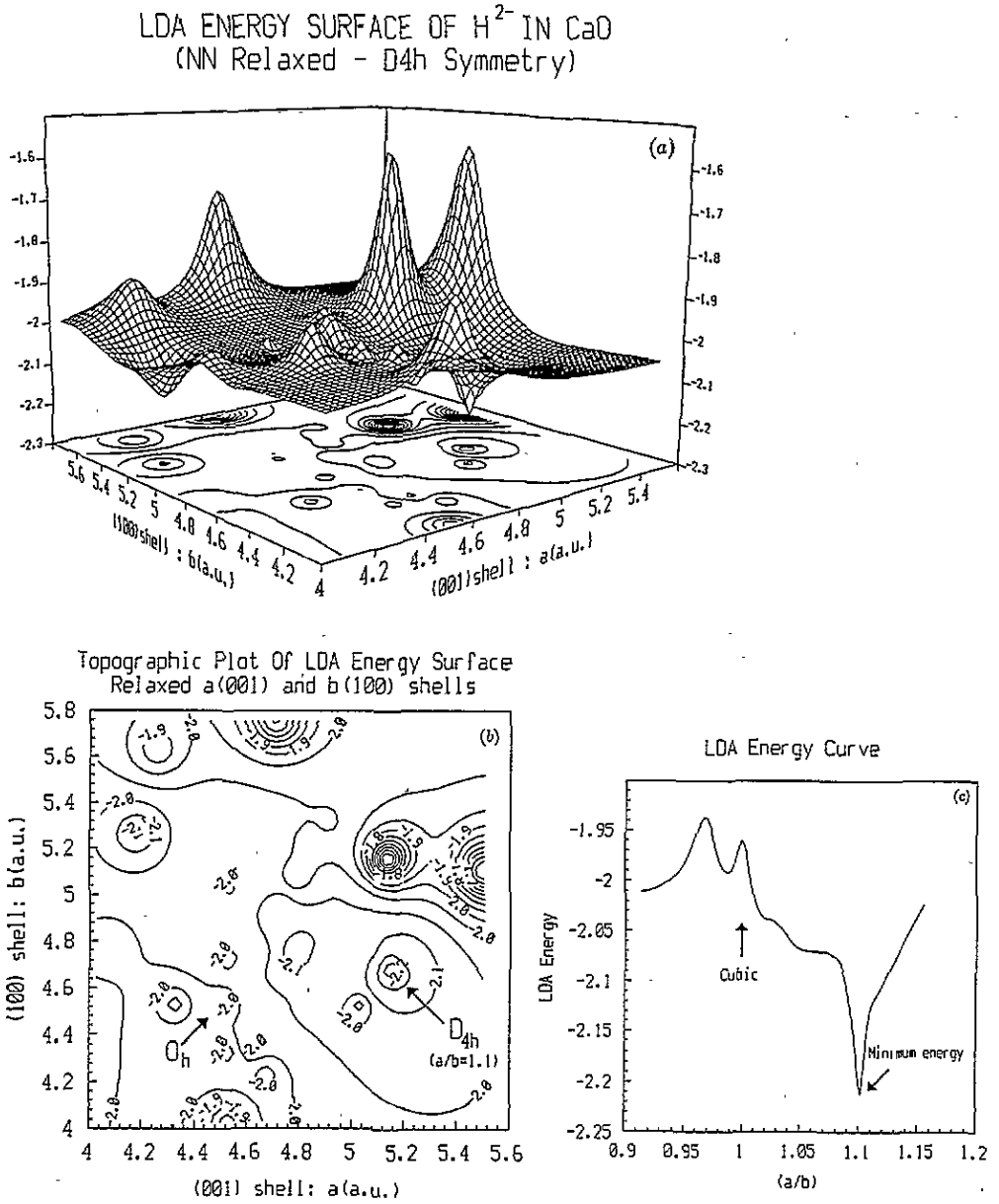

Figure 3. (a) The LDA total energy surface of an H^{2-} ion in CaO with the six nearest-neighbour Ca^{2+} nuclei relaxed in local D_{4h} symmetry. The energy is plotted versus a and b, the shell parameters for the first and second atomic shells, with Ca^{2+} nuclei at the $a(001)$ and $b(100)$ sites. The remaining shell parameters are fixed at the bulk atomic spacing of 4.528 au. For clarity, the energies in au are expressed relative to −10 800 au. (b) Topographic plots of the energy surface from (a). The energy values shown along the contours are offset by −10 800 au. The experimental and extreme energy minimum geometry are designated as O_h and D_{4h} respectively. (c) The LDA total energy versus distortion curve for figure 3(a). The curve is generated by intersecting the 3D surface with an energy plane connecting the starting geometry O_h and the energy minimum geometry D_{4h}. The distortion axis is expressed as a ratio (a/b) of the H–Ca(001) bond length versus H–Ca(100). The extreme energy minimum is obvious.

Table 3. *Hyperfine and superhyperfine Fermi contact interactions for H^{2-} in CaO.*

	Spin density in units of 10^{20} cm^{-3}			
	H	Ca(100)	Ca(001)	Reference
H^{2-} in point-charge potential	706			This work
H^{2-} in CaO of O_h symmetry	270	3375	3375	This work
H^{2-} in CaO of D_{4h} symmetry	283	201	−7520	This work
Experimental results (D_{4h})	420	2330		[5]

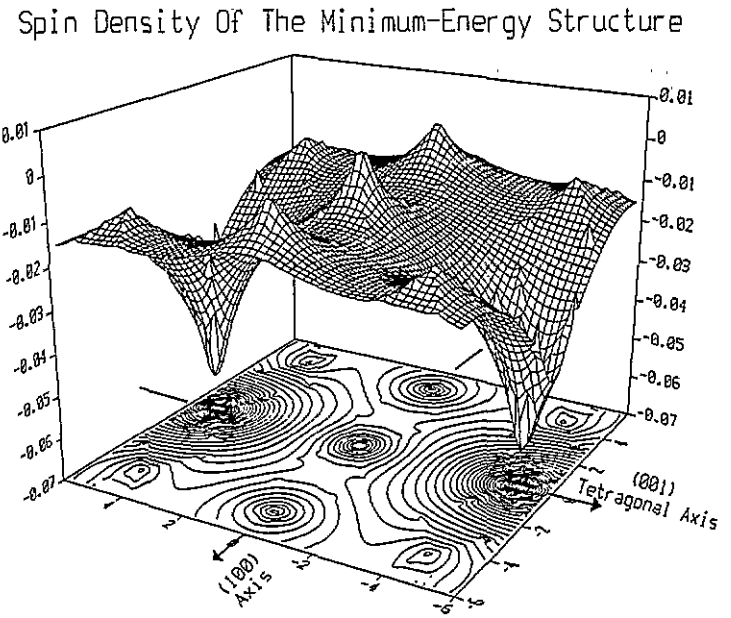

Figure 4. The unpaired spin density plot of the [010] plane in extreme energy minimum configuration. The spin density is in units of spin Bohr^{-3}. Values of spin densities at the proton and the Ca^{2+} nuclei at the (100) and (001) sites are listed in table 3. The geographic centre is the H^{2-} ion, which is surrounded by four Ca^{2+} nuclei located along the crystal axis and four O^{2-} nuclei located at the corners of the graph.

To investigate the origin of spin density at the proton, we replaced the Ca and O ions surrounding the H^{2-} ion with point charges to eliminate the unpaired density arising from the pure overlap effect, that is the H^{2-} ion is embedded in the Madelung potential only. In this case, we find the spin density at the proton is 706×10^{20} cm^{-3}. A Mulliken analysis indicates that the first two electrons of H^{2-} are located on the hydrogen 1s-like orbital and the third electron is located on the 2p-like orbital. Since the p orbital contributes no Fermi contact interaction at the proton, we can then conjecture that the spin density at the proton is due to the core polarization of the 1s shell by exchange with the 2p electron. Consequently, we obtain a finite difference of the electron densities at the nucleus which leads to the hyperfine interaction of contact character as

$$H = \left(\frac{8\pi}{3}\right)\beta_e[\phi^2_{1s\uparrow}(0) - \phi^2_{1s\downarrow}(0)].$$

Here $\phi^2_{1s\uparrow}(0)$ is the orbital wavefunction for the 1s shell of majority spin, and $\phi^2_{1s\downarrow}(0)$ for the

minority spin. Now an explanation of the decrease in spin densities at the proton on going from an isolated H^{2-} ion in Madelung potential to that in a CaO host is that the crystal field of surrounding Ca ions admixes d states into the 2p hydrogen ground state (table 2), decreasing the amount of core polarization as the 2p electron spreads out.

The spin densities on the proton and on the four calcium nuclei in the [100] plane containing the elongated axis (001) is illustrated in figure 4 and compared with experimental results in table 3. Our calculation shows a very good agreement of spin densities with experimental values at the proton in both O_h and D_{4h} symmetry. For spin densities at the calcium nuclei as calculated in the extreme minimum-energy configuration, a remarkable reduction of spin densities on the (100) calcium nuclei is found (10% of the experimental values); and a significiant discrepancy exists between the calculated value and the undetected superhyperfine interaction with the (001) calcium nuclei. However, it is important to point out how the spin densities vary with response to the lattice distortion. In O_h symmetry the calculated spin density at the calcium nuclei is 3375×10^{20} cm^{-3}, which is comparable with the experimental finding of 2330×10^{20} cm^{-3} at the (100) calcium nuclei in D_{4h} symmetry. The process of going from 3375×10^{20} to 201×10^{20} cm^{-3} at the (100) calcium sites, as calculated in a relaxed cluster of O_h and D_{4h} respectively, indicates a high sensitivity of the spin density to the lattice relaxation. Consequently, this lattice relaxation process produces a change from 3375×10^{20} to -7520×10^{20} cm^{-3} at the (001) calcium sites. We have not been able to give a complete analysis on this peculiar charge transfer mechanism due to the lattice relaxation. We also note Vail's work [16] on H^{2-} in MgO, where the spin densities on the nearest-neighbour Mg^{2+} nuclei are only 2% of the experimental value, showing that this sort of discrepancy between theory and experiment is not without precedence.

Acknowledgments

We are grateful to Dr M R Pederson for providing his excellent computer code. We also thank Dr E G Bradford for providing technical assistance and acknowledge the Alabama Supercomputer Authority for a grant of CPU time on the Cray C90 at the Alabama Supercomputer Center where the calculations were carried out. One of us (DCP) acknowledges the financial support of the Alabama DOE/EPSCoR program.

References

[1] Orera V M and Chen Y 1987 *Phys. Rev.* B **36** 6120
[2] Tombrello J, Tohver H T, Chen Y and Wilson T M 1984 *Phys. Rev.* **30** 7374
[3] Orera V M and Chen Y 1987 *Phys. Rev.* B **36** 1244
[4] Orera V M, Sanjuan M L and Chen Y 1991 *Phys. Rev.* B **42** 7604
[5] Ke S C and Tohver H T 1995 *Phys. Rev.* B **52** 9387
[6] Hsu J W 1991 *PhD thesis* University of Alabama
[7] Room T 1993 *PhD thesis* University of Tartunsis
[8] Hohenberg P and Kohn W 1965 *Phys. Rev.* **136** B864
Kohn W and Sham L J 1965 *Phys. Rev.* **140** A1133
[9] Jackson K, Pederson M R and Harrison J G 1990 *Phys. Rev.* B **41** 12 641
[10] Frank F C 1950 *Phil. Mag.* **41** 1287
[11] Jackson K and Pederson M R 1990 *Phys. Rev.* B **42** 3276
[12] *Almanac of Bruker Analytical Instruments* 1994 p 118
[13] Perdew J P and Zunger A 1981 *Phys. Rev.* B **23** 5048
[14] Whited R O and Walker W C 1969 *Phys. Rev.* **188** 1380
[15] Lobatch V A and Rubin I R 1990 *Phys. Status Solidi* b **160** 505
[16] Vail J M 1990 *J. Phys. Chem. Solids* **51** 589